DESY–09–137
September, 2009

arXiv:0910.1235v2 [hep-ex] 23 Jun 2010

Measurement of J/ψ photoproduction at large momentum transfer at HERA

ZEUS Collaboration

Abstract

The proton-dissociative diffractive photoproduction of J/ψ mesons has been studied in ep collisions with the ZEUS detector at HERA using an integrated luminosity of 112 pb^{-1}. The cross section is presented as a function of the photon-proton centre-of-mass energy and of the squared four-momentum transfer at the proton vertex. The results are compared to perturbative QCD calculations.

The ZEUS Collaboration

S. Chekanov, M. Derrick, S. Magill, B. Musgrave, D. Nicholass[1], J. Repond, R. Yoshida
Argonne National Laboratory, Argonne, Illinois 60439-4815, USA [n]

M.C.K. Mattingly
Andrews University, Berrien Springs, Michigan 49104-0380, USA

P. Antonioli, G. Bari, L. Bellagamba, D. Boscherini, A. Bruni, G. Bruni, F. Cindolo, M. Corradi, G. Iacobucci, A. Margotti, R. Nania, A. Polini
INFN Bologna, Bologna, Italy [e]

S. Antonelli, M. Basile, M. Bindi, L. Cifarelli, A. Contin, S. De Pasquale[2], G. Sartorelli, A. Zichichi
University and INFN Bologna, Bologna, Italy [e]

D. Bartsch, I. Brock, H. Hartmann, E. Hilger, H.-P. Jakob, M. Jüngst, A.E. Nuncio-Quiroz, E. Paul, U. Samson, V. Schönberg, R. Shehzadi, M. Wlasenko
Physikalisches Institut der Universität Bonn, Bonn, Germany [b]

J.D. Morris[3]
H.H. Wills Physics Laboratory, University of Bristol, Bristol, United Kingdom [m]

M. Kaur, P. Kaur[4], I. Singh[4]
Panjab University, Department of Physics, Chandigarh, India

M. Capua, S. Fazio, A. Mastroberardino, M. Schioppa, G. Susinno, E. Tassi[5]
Calabria University, Physics Department and INFN, Cosenza, Italy [e]

J.Y. Kim[6]
Chonnam National University, Kwangju, South Korea

Z.A. Ibrahim, F. Mohamad Idris, B. Kamaluddin, W.A.T. Wan Abdullah
Jabatan Fizik, Universiti Malaya, 50603 Kuala Lumpur, Malaysia [r]

Y. Ning, Z. Ren, F. Sciulli
Nevis Laboratories, Columbia University, Irvington on Hudson, New York 10027, USA [o]

J. Chwastowski, A. Eskreys, J. Figiel, A. Galas, K. Olkiewicz, B. Pawlik, P. Stopa, L. Zawiejski
The Henryk Niewodniczanski Institute of Nuclear Physics, Polish Academy of Sciences, Cracow, Poland [i]

L. Adamczyk, T. Bołd, I. Grabowska-Bołd, D. Kisielewska, J. Łukasik[7], M. Przybycień, L. Suszycki
Faculty of Physics and Applied Computer Science, AGH-University of Science and Technology, Cracow, Poland [p]

A. Kotański[8], W. Słomiński[9]
Department of Physics, Jagellonian University, Cracow, Poland

O. Bachynska, O. Behnke, J. Behr, U. Behrens, C. Blohm, K. Borras, D. Bot, R. Ciesielski, N. Coppola, S. Fang, A. Geiser, P. Göttlicher[10], J. Grebenyuk, I. Gregor, T. Haas, W. Hain, A. Hüttmann, F. Januschek, B. Kahle, I.I. Katkov[11], U. Klein[12], U. Kötz, H. Kowalski, V. Libov, M. Lisovyi, E. Lobodzinska, B. Löhr, R. Mankel[13], I.-A. Melzer-Pellmann, S. Miglioranzi[14], A. Montanari, T. Namsoo, D. Notz, A. Parenti, P. Roloff, I. Rubinsky, U. Schneekloth, A. Spiridonov[15], D. Szuba[16], J. Szuba[17], T. Theedt, J. Tomaszewska[18], G. Wolf, K. Wrona, A.G. Yagües-Molina, C. Youngman, W. Zeuner[13]
Deutsches Elektronen-Synchrotron DESY, Hamburg, Germany

V. Drugakov, W. Lohmann, S. Schlenstedt
Deutsches Elektronen-Synchrotron DESY, Zeuthen, Germany

G. Barbagli, E. Gallo
INFN Florence, Florence, Italy [e]

P. G. Pelfer
University and INFN Florence, Florence, Italy [e]

A. Bamberger, D. Dobur, F. Karstens, N.N. Vlasov[19]
Fakultät für Physik der Universität Freiburg i.Br., Freiburg i.Br., Germany [b]

P.J. Bussey, A.T. Doyle, M. Forrest, D.H. Saxon, I.O. Skillicorn
Department of Physics and Astronomy, University of Glasgow, Glasgow, United Kingdom [m]

I. Gialas[20], K. Papageorgiu
Department of Engineering in Management and Finance, Univ. of the Aegean, Chios, Greece

U. Holm, R. Klanner, E. Lohrmann, H. Perrey, P. Schleper, T. Schörner-Sadenius, J. Sztuk, H. Stadie, M. Turcato
Hamburg University, Institute of Exp. Physics, Hamburg, Germany [b]

K.R. Long, A.D. Tapper
Imperial College London, High Energy Nuclear Physics Group, London, United Kingdom [m]

T. Matsumoto[21], K. Nagano, K. Tokushuku[22], S. Yamada, Y. Yamazaki[23]
Institute of Particle and Nuclear Studies, KEK, Tsukuba, Japan [f]

A.N. Barakbaev, E.G. Boos, N.S. Pokrovskiy, B.O. Zhautykov
Institute of Physics and Technology of Ministry of Education and Science of Kazakhstan, Almaty, Kazakhstan

V. Aushev[24], M. Borodin, I. Kadenko, Ie. Korol, O. Kuprash, D. Lontkovskyi, I. Makarenko, Yu. Onishchuk, A. Salii, Iu. Sorokin, A. Verbytskyi, V. Viazlo, O. Volynets, O. Zenaiev, M. Zolko
Institute for Nuclear Research, National Academy of Sciences, and Kiev National University, Kiev, Ukraine

D. Son
Kyungpook National University, Center for High Energy Physics, Daegu, South Korea [g]

J. de Favereau, K. Piotrzkowski
Institut de Physique Nucléaire, Université Catholique de Louvain, Louvain-la-Neuve, Belgium [q]

F. Barreiro, C. Glasman, M. Jimenez, J. del Peso, E. Ron, J. Terrón, C. Uribe-Estrada
Departamento de Física Teórica, Universidad Autónoma de Madrid, Madrid, Spain [l]

F. Corriveau, J. Schwartz, C. Zhou
Department of Physics, McGill University, Montréal, Québec, Canada H3A 2T8 [a]

T. Tsurugai
Meiji Gakuin University, Faculty of General Education, Yokohama, Japan [f]

A. Antonov, B.A. Dolgoshein, D. Gladkov, V. Sosnovtsev, A. Stifutkin, S. Suchkov
Moscow Engineering Physics Institute, Moscow, Russia [j]

R.K. Dementiev, P.F. Ermolov [†], L.K. Gladilin, Yu.A. Golubkov, L.A. Khein, I.A. Korzhavina, V.A. Kuzmin, B.B. Levchenko[25], O.Yu. Lukina, A.S. Proskuryakov, L.M. Shcheglova, D.S. Zotkin
Moscow State University, Institute of Nuclear Physics, Moscow, Russia [k]

I. Abt, A. Caldwell, D. Kollar, B. Reisert, W.B. Schmidke
Max-Planck-Institut für Physik, München, Germany

G. Grigorescu, A. Keramidas, E. Koffeman, P. Kooijman, A. Pellegrino, H. Tiecke, M. Vázquez[14], L. Wiggers
NIKHEF and University of Amsterdam, Amsterdam, Netherlands [h]

N. Brümmer, B. Bylsma, L.S. Durkin, A. Lee, T.Y. Ling
Physics Department, Ohio State University, Columbus, Ohio 43210, USA [n]

A.M. Cooper-Sarkar, R.C.E. Devenish, J. Ferrando, B. Foster, C. Gwenlan[26], K. Horton[27], K. Oliver, A. Robertson, R. Walczak
Department of Physics, University of Oxford, Oxford United Kingdom [m]

A. Bertolin, F. Dal Corso, S. Dusini, A. Longhin, L. Stanco
INFN Padova, Padova, Italy [e]

R. Brugnera, R. Carlin, A. Garfagnini, S. Limentani
Dipartimento di Fisica dell' Università and INFN, Padova, Italy [e]

B.Y. Oh, A. Raval, J.J. Whitmore[28]
Department of Physics, Pennsylvania State University, University Park, Pennsylvania 16802, USA [o]

Y. Iga
Polytechnic University, Sagamihara, Japan [f]

G. D'Agostini, G. Marini, A. Nigro
Dipartimento di Fisica, Università 'La Sapienza' and INFN, Rome, Italy [e]

J.C. Hart
Rutherford Appleton Laboratory, Chilton, Didcot, Oxon, United Kingdom [m]

H. Abramowicz[29], R. Ingbir, S. Kananov, A. Levy, A. Stern
Raymond and Beverly Sackler Faculty of Exact Sciences, School of Physics, Tel Aviv University,
Tel Aviv, Israel [d]

M. Ishitsuka, T. Kanno, M. Kuze, J. Maeda
Department of Physics, Tokyo Institute of Technology, Tokyo, Japan [f]

R. Hori, N. Okazaki, S. Shimizu[14]
Department of Physics, University of Tokyo, Tokyo, Japan [f]

R. Hamatsu, S. Kitamura[30], O. Ota[31], Y.D. Ri[32]
Tokyo Metropolitan University, Department of Physics, Tokyo, Japan [f]

M. Costa, M.I. Ferrero, V. Monaco, R. Sacchi, V. Sola, A. Solano
Università di Torino and INFN, Torino, Italy [e]

M. Arneodo, M. Ruspa
Università del Piemonte Orientale, Novara, and INFN, Torino, Italy [e]

S. Fourletov[33], J.F. Martin, T.P. Stewart
Department of Physics, University of Toronto, Toronto, Ontario, Canada M5S 1A7 [a]

S.K. Boutle[20], J.M. Butterworth, T.W. Jones, J.H. Loizides, M. Wing
Physics and Astronomy Department, University College London, London, United Kingdom [m]

B. Brzozowska, J. Ciborowski[34], G. Grzelak, P. Kulinski, P. Łużniak[35], J. Malka[35], R.J. Nowak, J.M. Pawlak, W. Perlanski[35], A.F. Żarnecki
Warsaw University, Institute of Experimental Physics, Warsaw, Poland

M. Adamus, P. Plucinski[36], T. Tymieniecka[37]
Institute for Nuclear Studies, Warsaw, Poland

Y. Eisenberg, D. Hochman, U. Karshon
Department of Particle Physics, Weizmann Institute, Rehovot, Israel [c]

E. Brownson, D.D. Reeder, A.A. Savin, W.H. Smith, H. Wolfe
Department of Physics, University of Wisconsin, Madison, Wisconsin 53706, USA [n]

S. Bhadra, C.D. Catterall, G. Hartner, U. Noor, J. Whyte
Department of Physics, York University, Ontario, Canada M3J 1P3 [a]

[1] also affiliated with University College London, United Kingdom
[2] now at University of Salerno, Italy
[3] now at Queen Mary University of London, United Kingdom
[4] also working at Max Planck Institute, Munich, Germany
[5] also Senior Alexander von Humboldt Research Fellow at Hamburg University, Institute of Experimental Physics, Hamburg, Germany
[6] supported by Chonnam National University, South Korea, in 2009
[7] now at Institute of Aviation, Warsaw, Poland
[8] supported by the research grant No. 1 P03B 04529 (2005-2008)
[9] This work was supported in part by the Marie Curie Actions Transfer of Knowledge project COCOS (contract MTKD-CT-2004-517186)
[10] now at DESY group FEB, Hamburg, Germany
[11] also at Moscow State University, Russia
[12] now at University of Liverpool, United Kingdom
[13] on leave of absence at CERN, Geneva, Switzerland
[14] now at CERN, Geneva, Switzerland
[15] also at Institute of Theoretical and Experimental Physics, Moscow, Russia
[16] also at INP, Cracow, Poland
[17] also at FPACS, AGH-UST, Cracow, Poland
[18] partially supported by Warsaw University, Poland
[19] partially supported by Moscow State University, Russia
[20] also affiliated with DESY, Germany
[21] now at Japan Synchrotron Radiation Research Institute (JASRI), Hyogo, Japan
[22] also at University of Tokyo, Japan
[23] now at Kobe University, Japan
[24] supported by DESY, Germany
[25] partially supported by Russian Foundation for Basic Research grant No. 05-02-39028-NSFC-a
[26] STFC Advanced Fellow
[27] nee Korcsak-Gorzo
[28] This material was based on work supported by the National Science Foundation, while working at the Foundation.
[29] also at Max Planck Institute, Munich, Germany, Alexander von Humboldt Research Award
[30] now at Nihon Institute of Medical Science, Japan
[31] now at SunMelx Co. Ltd., Tokyo, Japan
[32] now at Osaka University, Osaka, Japan
[33] now at University of Bonn, Germany
[34] also at Łódź University, Poland

[35] member of Łódź University, Poland
[36] now at Lund University, Lund, Sweden
[37] also at University of Podlasie, Siedlce, Poland
† deceased

[a] supported by the Natural Sciences and Engineering Research Council of Canada (NSERC)

[b] supported by the German Federal Ministry for Education and Research (BMBF), under contract Nos. 05 HZ6PDA, 05 HZ6GUA, 05 HZ6VFA and 05 HZ4KHA

[c] supported in part by the MINERVA Gesellschaft für Forschung GmbH, the Israel Science Foundation (grant No. 293/02-11.2) and the US-Israel Binational Science Foundation

[d] supported by the Israel Science Foundation

[e] supported by the Italian National Institute for Nuclear Physics (INFN)

[f] supported by the Japanese Ministry of Education, Culture, Sports, Science and Technology (MEXT) and its grants for Scientific Research

[g] supported by the Korean Ministry of Education and Korea Science and Engineering Foundation

[h] supported by the Netherlands Foundation for Research on Matter (FOM)

[i] supported by the Polish State Committee for Scientific Research, project No. DESY/256/2006 - 154/DES/2006/03

[j] partially supported by the German Federal Ministry for Education and Research (BMBF)

[k] supported by RF Presidential grant N 1456.2008.2 for the leading scientific schools and by the Russian Ministry of Education and Science through its grant for Scientific Research on High Energy Physics

[l] supported by the Spanish Ministry of Education and Science through funds provided by CICYT

[m] supported by the Science and Technology Facilities Council, UK

[n] supported by the US Department of Energy

[o] supported by the US National Science Foundation. Any opinion, findings and conclusions or recommendations expressed in this material are those of the authors and do not necessarily reflect the views of the National Science Foundation.

[p] supported by the Polish Ministry of Science and Higher Education as a scientific project (2009-2010)

[q] supported by FNRS and its associated funds (IISN and FRIA) and by an Inter-University Attraction Poles Programme subsidised by the Belgian Federal Science Policy Office

[r] supported by an FRGS grant from the Malaysian government

1 Introduction

Photoproduction of vector mesons (VMs) is usually thought of as a process where the photon fluctuates into a $q\bar{q}$ state, which then interacts with the proton and becomes a VM. If the spatial configuration of the $q\bar{q}$ state is large, its interaction with the proton is soft in nature and is usually described by Regge theory [1] together with the vector dominance model [2]. This applies to exclusive photoproduction of the light VMs ρ, ω and ϕ (see Ivanov, Nikolaev and Savin [3] for a recent review). For heavy VMs, the $q\bar{q}$ pair is squeezed into a small configuration and perturbative QCD (pQCD) [4] can be applied. In exclusive photoproduction of J/ψ, $\gamma\, p \to J/\psi\, p$, the mass of the J/ψ provides a hard scale at the photon vertex and the small-size $q\bar{q}$ pair interacts through a two-gluon ladder with partons in the proton. If the four-momentum-transfer squared at the proton vertex is small, $|t| \lesssim 1\,\mathrm{GeV}^2$, and the proton stays intact, the cross section is predicted to fall exponentially with $|t|$.

When $|t|$ increases, $|t| > 1\,\mathrm{GeV}^2$, the dominant process is that where the proton dissociates into a low-mass nucleon state Y,

$$\gamma\, p \to J/\psi\, Y. \tag{1}$$

At large $|t|$ values, the cross section is expected to have a power-law decrease with $|t|$ [5–8]. In addition, J/ψ photoproduction at large $|t|$ is a two-scale process in which the large mass of the heavy VM is the hard scale at the photon vertex and t is the hard scale at the proton vertex. At high photon-proton centre-of-mass energies, W, this process should be sensitive to BFKL [9] dynamics.

This paper contains results for the kinematic range $30 < W < 160\,\mathrm{GeV}$ and $2 < |t| < 20\,\mathrm{GeV}^2$, which is larger than for the previous ZEUS measurement [10]. The sample under study also represents more than a five-fold increase in integrated luminosity.

2 Experimental set-up

This analysis is based on data collected with the ZEUS detector at HERA in 1996−2000. In those years HERA operated with an electron[1] beam energy of 27.5 GeV and a proton beam energy, E_p, of 820 GeV (1996−1997) and 920 GeV (1998−2000). The data sample corresponds to an integrated luminosity of $112\,\mathrm{pb}^{-1}$, $36\,\mathrm{pb}^{-1}$ with $E_p = 820\,\mathrm{GeV}$ and $76\,\mathrm{pb}^{-1}$ with $E_p = 920\,\mathrm{GeV}$.

A detailed description of the ZEUS detector can be found elsewhere [11]. A brief outline of the components that are most relevant for this analysis is given below.

[1] Electrons and positrons are both referred to as electrons in this paper.

Charged particles were tracked in the central tracking detector (CTD) [12], which operated in a magnetic field of 1.43 T provided by a thin superconducting coil. The CTD consisted of 72 cylindrical drift chamber layers, organised in 9 superlayers covering the polar-angle[2] region $15^\circ < \theta < 164^\circ$. The transverse-momentum resolution for full-length tracks was $\sigma(p_T)/p_T = 0.0058p_T \oplus 0.0065 \oplus 0.0014/p_T$, with p_T in GeV. The high-resolution uranium–scintillator calorimeter (CAL) [13] consisted of three parts: the forward (FCAL), the barrel (BCAL) and the rear (RCAL) calorimeters. Each part was subdivided transversely into towers and longitudinally into one electromagnetic section (EMC) and either one (in RCAL) or two (in BCAL and FCAL) hadronic sections (HAC). The smallest subdivision of the calorimeter is called a cell. The CAL energy resolutions, as measured under test-beam conditions, were $\sigma(E)/E = 0.18/\sqrt{E}$ for electrons and $\sigma(E)/E = 0.35/\sqrt{E}$ for hadrons, with E in GeV.

The muon system [14] consisted of tracking detectors (forward, barrel and rear muon chambers: FMUON, B/RMUON), which were placed inside and outside a magnetised iron yoke surrounding the CAL. The inner chambers, F/B/RMUI, covered the polar angles from 10° to 34°, from 34° to 135° and from 135° to 171°, respectively.

The luminosity was determined from the rate of the bremsstrahlung process $ep \to e\gamma p$, where the photon was measured by a lead-scintillator calorimeter [15] located at $Z = -107\,\mathrm{m}$.

3 Kinematics and reconstruction

The proton-dissociative J/ψ production process in ep interactions,

$$e(k)p(P) \to e(k')J/\psi(v)Y(P'),$$

is illustrated in Fig. 1. The signature of these events consists of two oppositely charged muons from the J/ψ decay and of the remnant of the dissociated proton. In the case of photoproduction, the beam electron is scattered at small angles and escapes undetected down the beampipe.

The variables k, k', P, P' and v are the four-momenta of the incident electron, scattered electron, incident proton, diffractive nucleonic system Y and J/ψ, respectively. The four-momentum of the exchanged photon is denoted by q. The kinematic variables are the following:

[2] The ZEUS coordinate system is a right-handed Cartesian system, with the Z axis pointing in the proton beam direction, referred to as the "forward direction", and the X axis pointing towards the centre of HERA. The coordinate origin is at the nominal interaction point.

- $Q^2 = -q^2 = -(k-k')^2$, the negative squared four-momentum of the exchanged photon;
- $W^2 = (q+P)^2$, the squared centre-of-mass energy of the photon-proton system;
- $t = (P-P')^2 = (q-v)^2$, the squared four-momentum transfer at the proton vertex;
- $y = (P \cdot q)/(P \cdot k)$, the fraction of the electron energy transferred to the photon in the rest frame of the proton;
- $z = (P \cdot v)/(P \cdot q)$, the event inelasticity, i.e. the fraction of the virtual photon energy transferred to the J/ψ in the proton rest frame.

The dissociated proton either escapes undetected down the beampipe or deposits only a part of its energy in the CAL and hence the mass of the proton remnant, M_Y, cannot be measured precisely. However, M_Y is related to other kinematic variables through $M_Y^2 = W^2(1-z) - |t|$.

The following angles are used to describe the decay of the J/ψ (see Fig. 2):

- Φ, the angle between the electron-scattering plane and the vector-meson plane, in the photon-proton centre-of-mass frame;
- θ_h and ϕ_h, the polar and azimuthal angles of the positively-charged decay particle in the helicity frame. Here, the helicity frame is the J/ψ rest frame and the quantisation axis is the meson direction in the photon-proton centre-of-mass system. The polar angle, θ_h, is defined as the angle between the direction of the positively charged decay particle and the quantisation axis. The azimuthal angle, ϕ_h, is the angle between the decay plane and the vector-meson production plane.

In this study, photoproduction is characterised by the non-observation of the scattered electron. Thus, Q^2 ranges from the kinematic minimum, $Q^2_{\text{min}} = m_e^2 y^2/(1-y) \approx 10^{-7}\,\text{GeV}^2$, where m_e is the electron mass, up to $Q^2_{\text{max}} \approx 1\,\text{GeV}^2$, the value at which the scattered electron becomes observable in the CAL. Since the mean Q^2 is small, $\langle Q^2 \rangle \approx 5 \cdot 10^{-5}\,\text{GeV}^2$, it was neglected in the reconstruction of the other kinematic variables.

The variable t can be expressed as $t \approx -p_T^2$, where p_T is the transverse momentum of the produced vector meson in the laboratory frame. The variable W is calculated as $W^2 \approx 2E_p(E-p_Z)_{J/\psi}$, where E is the energy and p_Z is the longitudinal momentum of the vector meson. The quantities $(E-p_Z)_{J/\psi}$ and t were reconstructed using only the measured momenta of the VM muon decay particles.

The inelasticity z was computed from $z = (E-p_Z)_{J/\psi}/\sum(E-p_Z)$, where $\sum(E-p_Z) = (E-p_Z)_{J/\psi} + \sum(E-p_Z)_{\text{had}}$ and $\sum(E-p_Z)_{\text{had}}$ is reconstructed by summing over all the CAL energy deposits (larger than 300 MeV) not associated with the J/ψ candidate.

4 Event selection

The events were selected online by the ZEUS three-level trigger system [11, 16]. The events were required to have at least one track in the CTD. At least one track had to point towards a CAL energy deposit compatible with a minimum ionising particle as well as a signal in the inner muon chambers.

The following was required offline:

- no scattered electron observed;
- two tracks with opposite charge pointing to a primary vertex with $|Z_{\rm vertex}| < 50\,{\rm cm}$;
- both tracks well reconstructed, i.e. traversing at least three superlayers in the CTD, including the innermost layer;
- each track associated with a distinct CAL energy deposit within a radius of 30 cm;
- azimuthal angle between the two tracks associated with the two muon candidates less than 174° in order to reject cosmic-ray events;
- invariant mass of the two tracks, which were assigned a μ mass, in the range $2.6 < M_{\mu\mu} < 3.5\,{\rm GeV}$.

Events were required to be in a kinematic range where the properties of the final state particles were properly measured and the acceptance was well defined. This was satisfied for $2 < |t| < 20\,{\rm GeV}^2$ and $30 < W < 160\,{\rm GeV}$. The cut of $|t| > 2\,{\rm GeV}^2$ also significantly reduced the background from the exclusive process. A cut of $z > 0.95$ was applied to suppress non-diffractive background. This cut also restricted the invariant mass of the Y system to $M_Y < 30\,{\rm GeV}$.

The energy range $30 < W < 40\,{\rm GeV}$ was mainly populated by events triggered by the FMUON detector, while the range $40 < W < 160\,{\rm GeV}$ was dominated by B/RMUON-triggered events. The FMUON-triggered sample was limited to the data collected in 1996−1997 and covered the $|t|$ region up to $10\,{\rm GeV}^2$.

After this selection procedure the number of observed di-muon events was 2817.

5 Theoretical predictions

The reaction $\gamma\, p \to J/\psi\, Y$ can be viewed as a three-step process. The photon fluctuates into a $q\bar{q}$ pair that scatters off a single parton in the proton by the exchange of a colour singlet. The scattered $q\bar{q}$ pair becomes a J/ψ and the struck parton and the proton remnant together fragment into the system Y. In lowest-order QCD the colour singlet

exchanges a pair of gluons. In the leading logarithmic (LL) approximation, the process is described by the effective exchange of a gluon ladder.

As stated in the introduction, the process under study has two scales. At the photon vertex, where the photon fluctuates into a $q\bar{q}$ pair, the size is fixed and determined by the J/ψ mass. The second scale, $|t|$, controls the size of the system which emits the gluon ladder.

In the region where the scale $|t|$ is smaller than $M^2_{J/\psi}$ ($2 < |t| < 10\,\mathrm{GeV}^2$), the momenta on the gluon ladder are still expected to be ordered and thus a DGLAP [17] approach is appropriate. A calculation in this kinematic region has been carried out by Gotsman, Levin, Maor and Naftali (GLMN) [18], using their screening correction formalism and evolving the gluon in a LL DGLAP mechanism.

As $|t|$ increases, the BFKL mechanism is expected to dominate. The first LL BFKL calculations [5–7] were made using the Mueller-Tang (MT) approximation [19], which is only good for very large rapidity intervals. Enberg, Motyka and Poludniowski (EMP) [8] do not use the MT approximation and provide a complete analytical solution in LL for the case of heavy quarks (the case for any quark mass is discussed elsewhere [20, 21]). They use two different values of α_S as the pre-factor of the cross section and as the coupling relevant for the BFKL ladder. Enberg at al. [8] also present results of a non-leading (nonL) BFKL calculation.

In addition, a recent QCD calculation by Frankfurt, Strikman and Zhalov (FSZ) [22, 23] is motivated by the QCD factorisation theorem for large $|t|$ rapidity-gap processes and by the correspondence to exclusive J/ψ production at $|t| \sim 1\,\mathrm{GeV}^2$. In this QCD calculation in the triple-Pomeron limit, the W dependence of the cross section mainly depends on the gluon distribution of the proton.

In all models, a non-relativistic approximation of the J/ψ wave-function assuming equal sharing of longitudinal momenta between the quark and the anti-quark was used. The J/ψ retains the helicity of the photon which means that s-channel helicity is conserved (SCHC).

The DGLAP-motivated calculation predicts a mild W dependence of the cross section in the region of small $|t|$. In the region of larger $|t|$ the hard scale is chosen such that saturation is reached and thus the cross section is independent of W. The BFKL LL calculations predict a fast rise of the cross section with W which hardly depends on $|t|$. This is a unique feature of BFKL dynamics. The nonL BFKL model behaves in a similar way. In case of the FSZ parameterisation, the main energy dependence is provided by the behaviour of the gluon distribution.

All calculations predict an approximate power-law t-dependence of the cross section of the form $d\sigma/dt \sim |t|^{-n}$, where the value of n may depend on the $|t|$ range.

6 Monte Carlo and background evaluation

The acceptance and the effects of the detector response were determined using Monte Carlo (MC) events. All generated events were passed through the standard ZEUS detector simulation, based on GEANT 3.13 [24], the ZEUS trigger-simulation package and the same reconstruction and analysis programs as used for the data.

6.1 The process $ep \to e\ J/\psi\ Y$

The process $ep \to e\ J/\psi\ Y$ was modelled using the EPSOFT generator [25, 26]. The γp interactions were simulated assuming the exchange of a colourless object which couples to the whole proton, which subsequently fragments into a state Y. The particle multiplicities and the transverse momenta of the hadrons in the final state Y were simulated using parameterisations of pp data, while the longitudinal momenta were generated with a uniform rapidity distribution. The differential cross-section $d\sigma/dt$ was reweighted to obtain the shape observed in data. The assumption of s-channel helicity conservation was applied.

The differential cross section in M_Y^2 have the form $d\sigma/dM_Y^2 \propto (M_Y^2)^{-\beta(t,W)}$. The measured z distributions in $|t|$ and W bins were used to determine the $|t|$ and W dependence of the function $\beta(t, W)$. For each bin, a single value of the function β was extracted by using a χ^2 minimisation method. The results were parameterised in the form of $\beta(t, W) = (W/W_0)^{0.52\pm0.11} \exp((0.08 \pm 0.07) + (-0.14 \pm 0.03)|t|)$, with $W_0 = 95\,\text{GeV}$. This parameterisation was used in all further studies.

6.2 Evaluation of background

The main sources of background were the non-resonant QED $\gamma\gamma$ processes, misidentified pion production and resonant background produced through the decay of the $\psi(2S)$ meson.

The non-resonant background due to the QED Bethe-Heitler di-muon production, $ep \to e\mu^+\mu^- Y$, was simulated using the GRAPE-DILEPTON 1.1 generator [27]. The background from $\gamma\gamma \to \mu^+\mu^-$ events was estimated in each bin by normalising to the luminosity of the data. The contribution of this background increased with $|t|$ from 6 to 10%.

The $\psi(2S)$ background was estimated using the DIPSI generator [28]. This background was dominated by the processes $\psi \to J/\psi\pi^0\pi^0$ (BR=(17.51 ± 0.34)%) and $\psi \to \mu^+\mu^-$ (BR=(0.76 ± 0.08)%). It amounted to about 1% and 0.1%, respectively. The contribution

from $\psi \to J/\psi\pi^+\pi^-$ (BR=$(33.1 \pm 0.5)\%$) was strongly suppressed by selection criteria, i.e. a requirement of two-track events.

The background from exclusive J/ψ production was found [10] to be 5% for $2 < |t| < 3\,\mathrm{GeV}^2$. For $|t| > 3\,\mathrm{GeV}^2$, it was found to be consistent with zero. All background processes were subtracted bin-by-bin.

7 Systematic uncertainties

The systematic uncertainties were determined by varying the selection cuts and modifying the analysis procedure. Their effects on the integrated cross section are given in parentheses:

- the cut on Z vertex was changed by $\pm 10\,\mathrm{cm}$ ($+1.8\%$, -0.5%);
- the $\mu^+\mu^-$ mass window was changed to $2.8 - 3.4\,\mathrm{GeV}$ ($+0.2\%$);
- instead of using the MC to subtract the background bin-by-bin, it was fitted with a polynomial function and statistically subtracted ($+1.5\%$);
- the minimum energy of the CAL energy deposit included for the evaluation of the z variable was varied by $\pm 100\,\mathrm{MeV}$ ($+0.3\%$, -1.4%);
- the strategy of matching energy deposits to the decay tracks was changed. Instead of matching every object within 30 cm from the track, only one island within this distance was matched to the track (-0.7%);
- the uncertainty of the muon acceptance, including the detector, the trigger and the reconstruction efficiency, was obtained from a study [29] based on an independent dimuon sample ($\pm 6.3\%$);
- the uncertainty on the acceptance due to modelling of the hadronic final state in the EPSOFT MC was estimated by varying the parameter β within its errors ($\pm 2\%$).

The overall systematic uncertainty was determined by adding all the individual uncertainties in quadrature. The uncertainty on the luminosity measurement, 2%, was not included.

8 Results

8.1 The J/ψ signal

The invariant-mass distribution of the $\mu^+\mu^-$ pairs is presented in Fig. 3. A clear peak at the J/ψ mass is observed with very little non-resonant background.

The distributions of the kinematic variables $|t|$, W, z, ϕ_h and $\cos\theta_h$ are shown in Fig. 4. The MC distributions of the J/ψ events are shown as well as the QED background. The overall agreement between data and MC is good.

8.2 Determination of photon-proton cross-section

The ep cross section was determined by subtracting the background from the data, correcting for the acceptance, using the branching ratio for the muon channel decay ($5.88\pm0.10\%$) and using the measured luminosity.

Photon-proton cross sections were extracted from the ep cross sections by using photon flux factors. The flux factors [30] generated at the leptonic vertex relate the ep and the γp cross sections by

$$\frac{d^2\sigma^{ep\to eJ/\psi Y}}{dydQ^2} = \Gamma_T(y,Q^2)\sigma^{\gamma p}(y),$$

where Γ_T is the effective photon flux. The cross sections for different beam energies were averaged using the corresponding luminosities.

8.3 $|t|$ dependence

Differential γp cross section $d\sigma/dt$ for proton-dissociative J/ψ photoproduction was measured in the kinematic region $30 < W < 160\,\mathrm{GeV}$, $2 < |t| < 20\,\mathrm{GeV}^2$ and $z > 0.95$.

The differential cross section as a function of $|t|$ is shown in Fig. 5 and listed in Table 1. The cross section falls steeply with $|t|$. The data cannot be described in the whole $|t|$ region by one exponential function of the form $\sim e^{-b|t|}$, where b is a constant. Neither does a single power-law dependence of the form $|t|^{-n}$, where n is a constant, fit the data. A good fit can, however, be obtained by fitting two $|t|$ ranges separately, giving $n = 1.9\pm0.1$ for $2 < |t| < 5\,\mathrm{GeV}^2$ and $n = 3.0 \pm 0.1$ for $5 < |t| < 20\,\mathrm{GeV}^2$. Note that a good fit can also be obtained to a quadratic exponential function $e^{-b|t|+c|t|^2}$.

The differential cross-section $d\sigma/dt$ as a function of $|t|$ is shown again in Fig. 6, together with the H1 data [31], and compared with different theoretical models. The GLMN LL model gives a good description of the data up to about $|t| = 5\,\mathrm{GeV}^2$, but falls off slower than the data up to the region where the calculation is valid ($|t| < 10\,\mathrm{GeV}^2$). The EMP LL prediction, using $\alpha_S = 0.205$ in the pre-factor and $\alpha_S = 0.16$ in the BFKL evolution, lies below the data in the whole range of $|t|$. The FSZ results are shown for a calculation using a Pomeron trajectory with intercept of 1.1 and a slope of $0.005\,\mathrm{GeV}^{-2}$. Similar results are obtained with a Pomeron intercept of 1.0. The CTEQ6M parameterisation [32] of the parton density functions is used. The FSZ calculation describes the data well up to $|t|$ of about $12\,\mathrm{GeV}^2$ but falls-off too steeply at larger $|t|$ values.

8.4 W dependence

In the Regge formalism, the differential cross section can be expressed as

$$d\sigma/dt = F(t)W^{4(\alpha_{I\!P}(t)-1)}, \tag{2}$$

where $F(t)$ is a function of t and $\alpha_{I\!P}(t)$ is the effective Pomeron trajectory. This expression is usually used for exclusive reactions, but has been used also for the case where M_Y is integrated over [10, 31]. By studying the W dependence of $d\sigma/dt$ at fixed t, the Pomeron trajectory can be determined.

The W dependence of the differential cross section $d\sigma/dt$ for eight fixed t values is shown in Fig. 7 and listed in Table 2. At each t value the cross section is parameterised as $\sigma \sim W^{\delta}$ and the lines in the figure are the result of these fits. The values of $\alpha_{I\!P}$ can be obtained at each t value through

$$\alpha_{I\!P} = (\delta + 4)/4 \tag{3}$$

and are shown in Fig. 8. The values of δ and of $\alpha_{I\!P}$ are listed in Table 3. A linear fit of the form

$$\alpha_{I\!P}(t) = \alpha_{I\!P}(0) + \alpha'_{I\!P} \cdot t \tag{4}$$

yields an intercept

$$\alpha_{I\!P}(0) = 1.084 \pm 0.031(\text{stat.})^{+0.025}_{-0.018}(\text{syst.}), \tag{5}$$

and a slope

$$\alpha'_{I\!P} = -0.014 \pm 0.007(\text{stat.})^{+0.004}_{-0.005}(\text{syst.}). \tag{6}$$

The value of the intercept is consistent with that of the so-called "soft" Pomeron [33] (1.0808). The slope is different from that of the "soft" Pomeron [34] ($0.25\,\text{GeV}^{-2}$), but is consistent with the predictions of the BFKL Pomeron [35, 36].

The γp cross section as a function of W was measured in four bins of $|t|$: $2 < |t| < 3\,\text{GeV}^2$; $3 < |t| < 5\,\text{GeV}^2$; $5 < |t| < 10\,\text{GeV}^2$ and $10 < |t| < 20\,\text{GeV}^2$ for $30 < W < 160\,\text{GeV}$. The cross-section values are shown in Fig. 9 and summarised in Table 4. The H1 data [31] for the $|t|$ bin of 5 to $10\,\text{GeV}^2$ are also shown. A clear rise with W is seen in all the four $|t|$ regions. Also shown in the figure are the predictions of the models used in the comparison with $d\sigma/dt$. The DGLAP-based GLMN LL calculation agrees well with the data in the first two $|t|$ bins, but fails to describe the rise with W for $|t| > 5\,\text{GeV}^2$. The other two calculations, EMP LL and FSZ, predict a W dependence which is too steep in all the $|t|$ ranges presented in the analysis.

8.5 Decay angular distributions

The angular distributions of the J/ψ decay provide information about the photon and J/ψ polarisation states. The normalised two-dimensional angular distributions can be written in terms of spin density matrix elements, r, as:

$$\frac{1}{\sigma}\frac{d^2\sigma}{d\cos\theta_h d\phi_h} = \frac{3}{4\pi}\left(\frac{1}{2}(1+r_{00}^{04}) - \frac{1}{2}(3r_{00}^{04}-1)\cos^2\theta_h + \right.$$
$$\left. +\sqrt{2}\mathrm{Re}\{r_{10}^{04}\}\sin 2\theta_h\cos\phi_h + r_{1-1}^{04}\sin^2\theta_h\cos 2\phi_h\right). \quad (7)$$

The one-dimensional distributions result from the integration over θ_h or ϕ_h and are expressed as :

$$\frac{d\sigma}{d\cos\theta_h} \propto 1 + r_{00}^{04} + (1-3r_{00}^{04})\cos^2\theta_h \quad (8)$$

and

$$\frac{d\sigma}{d\phi} \propto 1 + r_{1-1}^{04}\cos 2\phi_h. \quad (9)$$

The spin density matrix element r_{00}^{04} represents the probability that the produced J/ψ has helicity zero, $\mathrm{Re}\{r_{10}^{04}\}$ is proportional to the single-flip amplitude and r_{1-1}^{04} is related to the interference between non-flip and double-flip amplitudes. If SCHC holds, the J/ψ retains the helicity of the almost real photon and all the three matrix elements are expected to be zero.

The distributions of $\cos\theta_h$ and ϕ_h after background subtraction and acceptance corrections in four $|t|$ bins and for $30 < W < 160$ GeV are shown in Fig. 10. They were fitted using formulae (8) and (9). The r_{00}^{04}, $\mathrm{Re}\{r_{10}^{04}\}$ and r_{1-1}^{04} spin density matrix elements were extracted from a two-dimensional χ^2 minimisation fit using Eq. (7) and are summarised in Table 5 and shown in Fig. 11. The H1 data [31] are also shown. The results for r_{00}^{04} and r_{1-1}^{04} are compatible with zero. The values obtained for $\mathrm{Re}\{r_{10}^{04}\}$ are not compatible with zero for $|t| < 10\,\mathrm{GeV}^2$, contrary to the expectation from SCHC.

The measurements of the present analysis, the differential cross section as a function of $|t|$, the W dependence of the cross section and the density matrix elements, are in good agreement with those of the H1 collaboration [31] within the common kinematic region.

9 Summary

Proton-dissociative J/ψ production was measured at HERA in the photoproduction regime in the kinematic region $30 < W < 160$ GeV, $z > 0.95$ and $2 < |t| < 20\,\mathrm{GeV}^2$.

The $|t|$ dependence of the differential cross section, $d\sigma/d|t|$, is found to be approximately power-like, $\sim |t|^{-n}$, with the power n increasing with $|t|$.

The effective Pomeron trajectory was derived from a measurement of the W dependence of the cross section at fixed t values. The value of the slope of the trajectory is compatible with zero. It is consistent with the predictions of the BFKL Pomeron but different from the slope of the "soft" Pomeron.

The cross-section $\sigma(\gamma p \to J/\psi\, Y)$ rises significantly with W in each $|t|$ bin. The t and W dependence of the cross section were compared to several theoretical calculations. The DGLAP-motivated GLMN LL [18] calculation can describe the behaviour of the data, both in t and in W, up to $|t| = 5\,\mathrm{GeV}^2$. The BFKL-motivated EMP LL [8] calculation fails to describe the data in the kinematic region of the present measurement. The FSZ [22,23] calculation describes the t dependence of the cross section only up to $|t| = 12\,\mathrm{GeV}^2$ and fails to reproduce the W dependence.

The spin density matrix elements of the J/ψ, r^{04}_{00} and r^{04}_{1-1} are consistent with zero, as expected from s-channel helicity conservation. The values obtained for $\mathrm{Re}\{r^{04}_{10}\}$ are not compatible with zero for $|t| < 10\,\mathrm{GeV}^2$, contrary to the expectation from SCHC.

Acknowledgments

We appreciate the contributions to the construction and maintenance of the ZEUS detector of many people who are not listed as authors. The HERA machine group and the DESY computing staff are especially acknowledged for their success in providing excellent operation of the collider and the data analysis environment. We thank the DESY directorate for their strong support and encouragement. We want to thank Asher Gotsman, Jeff Forshaw, Lonya Frankfurt, Uri Maor, Leszek Motyka and Mark Strikman for many useful discussions. We are grateful to Rikard Enberg, Eran Naftali and Michael Zhalov for providing the results of their theoretical calculations.

References

[1] P.D.B. Collins, *An Introduction to Regge Theory and High Energy Physics.* Cambridge University Press, 1977.

[2] J.J. Sakurai, Ann. Phys. **11**, 1 (1960);
J.J. Sakurai, Phys. Rev. Lett. **22**, 981 (1969).

[3] I.P. Ivanov, N.N. Nikolaev and A.A. Savin, Phys. Part. Nucl. **37**, 1 (2006).

[4] H. Abramowicz, L. Frankfurt and M. Strikman, Surveys High Energy Phys. **11**, 51 (1997).

[5] J.R. Forshaw and M.G. Ryskin, Z. Phys. **C 68**, 137 (1995).

[6] J. Bartels et al., Phys. Lett. **B 375**, 301 (1996).

[7] J.R. Forshaw and G. Poludniowski, Eur. Phys. J. **C 26**, 411 (2003).

[8] R. Enberg, L. Motyka and G. Poludniowski, Eur. Phys. J. **C 26**, 219 (2003).

[9] E.A. Kuraev, L.N. Lipatov and V.S. Fadin, Sov. Phys. JETP **44**, 443 (1976);
E.A. Kuraev, L.N. Lipatov and V.S. Fadin, Sov. Phys. JETP **45**, 199 (1977);
Ya.Ya. Balitskiĭ and L.N. Lipatov, Sov. J. Nucl. Phys. **28**, 822 (1978).

[10] ZEUS Coll., S. Chekanov et al., Eur. Phys. J. **C 26**, 389 (2003).

[11] ZEUS Coll., U. Holm (ed.), *The ZEUS Detector.* Status Report (unpublished), DESY (1993), available on `http://www-zeus.desy.de/bluebook/bluebook.html`.

[12] N. Harnew et al., Nucl. Inst. Meth. **A 279**, 290 (1989);
B. Foster et al., Nucl. Phys. Proc. Suppl. **B 32**, 181 (1993);
B. Foster et al., Nucl. Inst. Meth. **A 338**, 254 (1994).

[13] M. Derrick et al., Nucl. Inst. Meth. **A 309**, 77 (1991);
A. Andresen et al., Nucl. Inst. Meth. **A 309**, 101 (1991);
A. Caldwell et al., Nucl. Inst. Meth. **A 321**, 356 (1992);
A. Bernstein et al., Nucl. Inst. Meth. **A 336**, 23 (1993).

[14] G. Abbiendi et al., Nucl. Inst. Meth. **A 333**, 342 (1993).

[15] J. Andruszków et al., Acta Phys. Pol. **B 32**, 2025 (2001).

[16] W.H. Smith, K. Tokushuku and L.W. Wiggers, *Proc. Computing in High-Energy Physics (CHEP), Annecy, France, Sept. 1992*, C. Verkerk and W. Wojcik (eds.), p. 222. CERN, Geneva, Switzerland (1992). Also in preprint DESY 92-150B.

[17] V.N. Gribov and L.N. Lipatov, Sov. J. Nucl. Phys. **15**, 438 (1972);
V.N. Gribov and L.N. Lipatov, Sov. J. Nucl. Phys. **15**, 675 (1972);

Y.L. Dokshitzer, Sov. Phys. JETP **46**, 641 (1977);
G. Altareli and G. Parisi, Nucl. Phys. **B 126**, 298 (1977).

[18] E. Gotsman et al., Phys. Lett. **B 532**, 37 (2002).

[19] A.H. Mueller and W.-K. Tang, Phys. Lett. **B 284**, 123 (1992).

[20] R. Enberg et al., JHEP **0309**, 008 (2003).

[21] G. Poludniowski et al., JHEP **0312**, 002 (2003).

[22] L. Frankfurt, M. Strikman and M. Zhalov, Phys. Lett. **B 670**, 32 (2008).

[23] L. Frankfurt and M. Strikman, Phys. Rev. Lett. **63**, 1914 (1989).

[24] R. Brun et al., *GEANT 3.13*, 1987. CERN DD/EE/84-1.

[25] M. Kasprzak, *Inclusive properties of diffractive and nondiffractive photoproduction at HERA*. Ph.D. Thesis, Warsaw Univ., Warsaw, Poland, Report DESY F35D-96-16, 1996.

[26] L. Adamczyk, *Vector Meson Photoproduction at Large Momentum Transfer at HERA*. Ph.D. Thesis, Univ. of Mining and Metallurgy, Cracow, Poland, Report DESY-THESIS-1999-045, 1999.

[27] T. Abe, Comp. Phys. Comm. **136**, 126 (2001).

[28] M. Arneodo, L. Lamberti and M. Ryskin, Comp. Phys. Comm. **100**, 195 (1997).

[29] M. Turcato, *Open beauty photoproduction at HERA*. Ph.D. Thesis, Univ. of Padova, Padova, Italy, Report DESY-THESIS-2003-039, 2002.

[30] V.M. Budnev et al., Phys. Rep. **15C**, 181 (1974).

[31] H1 Coll., A. Aktas et al., Phys. Lett. **B 568**, 205 (2003).

[32] J. Pumplin et al., JHEP **0207**, 012 (2002).

[33] A. Donnachie and P.V. Landshoff, Phys. Lett. **B 296**, 227 (1992).

[34] A. Donnachie and P.V. Landshoff, Nucl. Phys. **B 231**, 189 (1984).

[35] S.J. Brodsky et al., JETP Lett. **70**, 155 (1999).

[36] N.N. Nikolaev, B.G. Zakharov and V.R. Zoller, Phys. Lett. **B 366**, 337 (1996).

$\|t\|$ bin (GeV^2)	$\langle\|t\|\rangle$ (GeV^2)	$d\sigma/d\|t\|$ ($\mathrm{nb}/\mathrm{GeV}^2$)
2.0 – 3.0	2.5	$6.05 \pm 0.23\ ^{+0.60}_{-0.43}$
3.0 – 4.0	3.5	$3.14 \pm 0.18\ ^{+0.29}_{-0.23}$
4.0 – 5.0	4.4	$1.91 \pm 0.13\ ^{+0.17}_{-0.18}$
5.0 – 6.5	5.6	$0.97 \pm 0.08\ ^{+0.11}_{-0.10}$
6.5 – 8.0	7.2	$0.41 \pm 0.05\ ^{+0.06}_{-0.03}$
8.0 – 11.0	9.3	$0.21 \pm 0.02\ ^{+0.04}_{-0.02}$
11.0 – 14.0	12.4	$0.07 \pm 0.01\ ^{+0.02}_{-0.01}$
14.0 – 20.0	16.5	$0.05 \pm 0.01\ ^{+0.01}_{-0.01}$

Table 1: *Differential cross-section $d\sigma/d|t|$ as a function of $|t|$ for $30 < W < 160$ GeV and $z > 0.95$. The first uncertainty is statistical and the second is systematic.*

$\lvert t\rvert$ bin (GeV^2)	$-t$ (GeV^2)	W bin (GeV)	$\langle W\rangle$ (GeV)	$d\sigma/dt$ (nb/ GeV^2)
2.0−2.5	2.2	30 − 50	39.5	$3.82 \pm 0.59\ ^{+0.68}_{-0.51}$
		50 − 70	59.5	$6.65 \pm 0.61\ ^{+0.58}_{-0.65}$
		70 − 80	75.0	$8.52 \pm 1.10\ ^{+0.90}_{-0.98}$
		80 − 90	84.8	$5.95 \pm 0.91\ ^{+0.65}_{-0.51}$
		90 − 100	95.0	$7.10 \pm 1.08\ ^{+0.57}_{-1.18}$
		100 − 110	105.1	$7.51 \pm 1.13\ ^{+0.89}_{-0.70}$
		110 − 120	114.9	$6.83 \pm 1.20\ ^{+0.99}_{-0.58}$
		120 − 130	125.1	$8.79 \pm 1.52\ ^{+0.98}_{-0.78}$
		130 − 160	144.0	$6.74 \pm 0.93\ ^{+1.25}_{-0.63}$
2.5−3.0	2.7	30 − 50	39.6	$2.47 \pm 0.52\ ^{+0.60}_{-0.31}$
		50 − 70	59.3	$3.93 \pm 0.50\ ^{+0.37}_{-0.53}$
		70 − 80	74.8	$5.43 \pm 0.91\ ^{+0.74}_{-0.91}$
		80 − 90	85.0	$4.52 \pm 0.84\ ^{+0.67}_{-0.73}$
		90 − 100	95.0	$4.89 \pm 0.93\ ^{+0.56}_{-0.32}$
		100 − 110	104.8	$4.81 \pm 0.95\ ^{+0.51}_{-0.53}$
		110 − 120	114.7	$6.02 \pm 1.26\ ^{+0.71}_{-0.64}$
		120 − 130	124.9	$6.34 \pm 1.33\ ^{+1.08}_{-0.65}$
		130 − 160	144.5	$7.00 \pm 1.17\ ^{+0.92}_{-0.68}$
3.0−4.0	3.4	30 − 50	39.7	$2.06 \pm 0.34\ ^{+0.29}_{-0.30}$
		50 − 70	59.5	$2.65 \pm 0.30\ ^{+0.23}_{-0.13}$
		70 − 80	74.8	$3.33 \pm 0.53\ ^{+0.30}_{-0.33}$
		80 − 90	84.8	$3.17 \pm 0.53\ ^{+0.34}_{-0.45}$
		90 − 110	99.8	$3.38 \pm 0.45\ ^{+0.36}_{-0.21}$
		110 − 130	119.6	$3.72 \pm 0.54\ ^{+0.32}_{-0.30}$
		130 − 160	143.5	$3.26 \pm 0.52\ ^{+0.49}_{-0.38}$

Table 2: *Differential cross section as a function of W in eight t bins and for $z > 0.95$. The first uncertainty is statistical and the second is systematic.*

$\lvert t\rvert$ bin (GeV^2)	$-t$ (GeV^2)	W bin (GeV)	$\langle W\rangle$ (GeV)	$d\sigma/dt$ ($\mathrm{nb}/\mathrm{GeV}^2$)
4.0−5.0	4.5	30 − 50	39.5	$0.95 \pm 0.23\ ^{+0.08}_{-0.18}$
		50 − 70	59.8	$1.51 \pm 0.22\ ^{+0.10}_{-0.17}$
		70 − 80	74.8	$1.97 \pm 0.38\ ^{+0.15}_{-0.22}$
		80 − 90	85.1	$1.98 \pm 0.39\ ^{+0.23}_{-0.34}$
		90 − 110	99.6	$1.71 \pm 0.29\ ^{+0.24}_{-0.30}$
		110 − 130	119.7	$2.44 \pm 0.44\ ^{+0.44}_{-0.29}$
		130 − 160	144.5	$2.82 \pm 0.51\ ^{+0.37}_{-0.52}$
5.0−6.5	5.7	30 − 70	48.1	$0.45 \pm 0.15\ ^{+0.08}_{-0.07}$
		50 − 70	59.6	$0.79 \pm 0.14\ ^{+0.11}_{-0.07}$
		70 − 90	79.9	$1.00 \pm 0.15\ ^{+0.12}_{-0.16}$
		90 − 110	100.0	$1.07 \pm 0.19\ ^{+0.12}_{-0.15}$
		110 − 160	134.1	$1.20 \pm 0.17\ ^{+0.17}_{-0.13}$
6.5−8.0	7.2	30 − 70	47.7	$0.17 \pm 0.11\ ^{+0.02}_{-0.02}$
		50 − 70	60.0	$0.28 \pm 0.08\ ^{+0.05}_{-0.08}$
		70 − 90	79.4	$0.22 \pm 0.07\ ^{+0.07}_{-0.01}$
		90 − 110	99.8	$0.43 \pm 0.11\ ^{+0.08}_{-0.06}$
		110 − 160	133.6	$0.64 \pm 0.13\ ^{+0.12}_{-0.06}$
8.0−11.0	9.2	50 − 70	59.5	$0.12 \pm 0.04\ ^{+0.03}_{-0.01}$
		70 − 90	80.4	$0.24 \pm 0.05\ ^{+0.05}_{-0.03}$
		90 − 110	99.6	$0.21 \pm 0.06\ ^{+0.05}_{-0.04}$
		110 − 160	133.4	$0.26 \pm 0.05\ ^{+0.04}_{-0.03}$
11.0−20.0	14.2	50 − 70	59.8	$0.04 \pm 0.01\ ^{+0.01}_{-0.01}$
		70 − 90	79.3	$0.05 \pm 0.01\ ^{+0.01}_{-0.01}$
		90 − 110	100.0	$0.07 \pm 0.02\ ^{+0.02}_{-0.02}$
		110 − 160	133.9	$0.07 \pm 0.02\ ^{+0.02}_{-0.01}$

Table 2 (Continuation): *Differential cross section as a function of W in eight t bins and for $z > 0.95$. The first uncertainty is statistical and the second is systematic.*

$\lvert t\rvert$ bin (GeV^2)	$-t$ (GeV^2)	δ	$\alpha_{I\!P}$
2.0 – 2.5	2.2	$0.38 \pm 0.10\ ^{+0.11}_{-0.06}$	$1.10 \pm 0.03\ ^{+0.03}_{-0.02}$
2.5 – 3.0	2.7	$0.70 \pm 0.15\ ^{+0.10}_{-0.10}$	$1.18 \pm 0.04\ ^{+0.02}_{-0.02}$
3.0 – 4.0	3.4	$0.39 \pm 0.13\ ^{+0.08}_{-0.07}$	$1.10 \pm 0.03\ ^{+0.02}_{-0.02}$
4.0 – 5.0	4.5	$0.72 \pm 0.18\ ^{+0.08}_{-0.07}$	$1.18 \pm 0.05\ ^{+0.02}_{-0.02}$
5.0 – 6.5	5.7	$0.70 \pm 0.21\ ^{+0.12}_{-0.12}$	$1.18 \pm 0.05\ ^{+0.03}_{-0.03}$
6.5 – 8.0	7.2	$1.38 \pm 0.46\ ^{+0.37}_{-0.24}$	$1.35 \pm 0.12\ ^{+0.09}_{-0.06}$
8.0 – 11.0	9.2	$0.78 \pm 0.38\ ^{+0.06}_{-0.12}$	$1.20 \pm 0.09\ ^{+0.02}_{-0.03}$
11.0 – 20.0	14.2	$0.82 \pm 0.44\ ^{+0.34}_{-0.08}$	$1.21 \pm 0.11\ ^{+0.09}_{-0.02}$

Table 3: *The values of the parameters δ and the effective Pomeron trajectory $\alpha_{I\!P}$ for eight fixed t values. The first uncertainty is statistical and the second is systematic.*

$\lvert t\rvert$ bin (GeV^2)	$-t$ (GeV^2)	W bin (GeV)	$\langle W\rangle$ (GeV)	$d\sigma/dt$ (nb/ GeV^2)
2−3	2.5	30 − 50	39.5	$3.23 \pm 0.40\ ^{+0.43}_{-0.33}$
		50 − 70	59.4	$5.35 \pm 0.40\ ^{+0.31}_{-0.34}$
		70 − 80	74.9	$7.13 \pm 0.72\ ^{+0.74}_{-0.49}$
		80 − 90	84.9	$5.30 \pm 0.62\ ^{+0.47}_{-0.50}$
		90 − 100	95.0	$6.04 \pm 0.71\ ^{+0.37}_{-0.45}$
		100 − 110	105.0	$6.28 \pm 0.75\ ^{+0.57}_{-0.37}$
		110 − 120	114.8	$6.42 \pm 0.86\ ^{+0.57}_{-0.41}$
		120 − 130	125.1	$7.52 \pm 1.00\ ^{+0.77}_{-0.60}$
		130 − 160	144.3	$6.80 \pm 0.72\ ^{+0.71}_{-0.57}$
3−5	3.8	30 − 50	39.7	$3.10 \pm 0.42\ ^{+0.21}_{-0.20}$
		50 − 70	59.6	$4.23 \pm 0.37\ ^{+0.22}_{-0.23}$
		70 − 80	74.9	$5.28 \pm 0.65\ ^{+0.31}_{-0.36}$
		80 − 90	84.9	$5.22 \pm 0.67\ ^{+0.48}_{-0.45}$
		90 − 100	94.9	$4.29 \pm 0.63\ ^{+0.41}_{-0.26}$
		100 − 110	105.0	$6.42 \pm 0.93\ ^{+0.68}_{-0.42}$
		110 − 120	115.0	$5.79 \pm 0.92\ ^{+0.39}_{-0.32}$
		120 − 130	125.0	$6.55 \pm 1.07\ ^{+0.54}_{-0.53}$
		130 − 160	143.9	$6.40 \pm 0.75\ ^{+0.77}_{-0.63}$
5−10	6.7	30 − 70	53.9	$1.69 \pm 0.20\ ^{+0.14}_{-0.14}$
		70 − 90	79.9	$2.36 \pm 0.28\ ^{+0.20}_{-0.25}$
		90 − 110	99.9	$2.69 \pm 0.35\ ^{+0.18}_{-0.23}$
		110 − 160	133.8	$3.61 \pm 0.36\ ^{+0.34}_{-0.28}$
10−20	13.3	50 − 80	63.9	$0.50 \pm 0.108\ ^{+0.05}_{-0.07}$
		80 − 120	98.8	$0.72 \pm 0.132\ ^{+0.07}_{-0.12}$
		120 − 160	139.8	$0.84 \pm 0.188\ ^{+0.14}_{-0.10}$

Table 4: *The cross-section $\sigma(\gamma p \to J/\psi\ Y)$ as a function of W in four $\lvert t\rvert$ bins and for $z > 0.95$. The first uncertainty is statistical and the second is systematic.*

$\lvert t\rvert$ bin (GeV^2)	$\langle\lvert t\rvert\rangle$ (GeV^2)	r^{04}_{1-1}	r^{04}_{00}	$Re\{r^{04}_{10}\}$
2 – 3	2.5	$0.005 \pm 0.064\ ^{+0.019}_{-0.024}$	$0.090 \pm 0.088\ ^{+0.009}_{-0.017}$	$0.117 \pm 0.061\ ^{+0.025}_{-0.019}$
3 – 5	3.8	$-0.206 \pm 0.072\ ^{+0.021}_{-0.037}$	$-0.030 \pm 0.100\ ^{+0.041}_{-0.083}$	$0.197 \pm 0.068\ ^{+0.046}_{-0.055}$
5 – 10	6.7	$0.003 \pm 0.106\ ^{+0.036}_{-0.016}$	$-0.033 \pm 0.147\ ^{+0.020}_{-0.042}$	$0.154 \pm 0.088\ ^{+0.016}_{-0.025}$
10 – 20	13.3	$-0.164 \pm 0.240\ ^{+0.108}_{-0.115}$	$-0.259 \pm 0.328\ ^{+0.081}_{-0.062}$	$-0.153 \pm 0.172\ ^{+0.062}_{-0.047}$

Table 5: *The spin density matrix elements for* $30 < W < 160$ *GeV and* $z > 0.95$. *The first uncertainty is statistical and the second is systematic.*

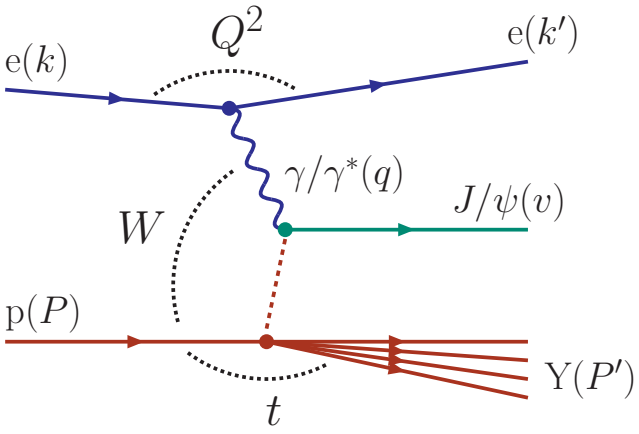

Figure 1: *Schematic diagram of proton-dissociative J/ψ production in ep interactions, $ep \to eJ/\psi\ Y$.*

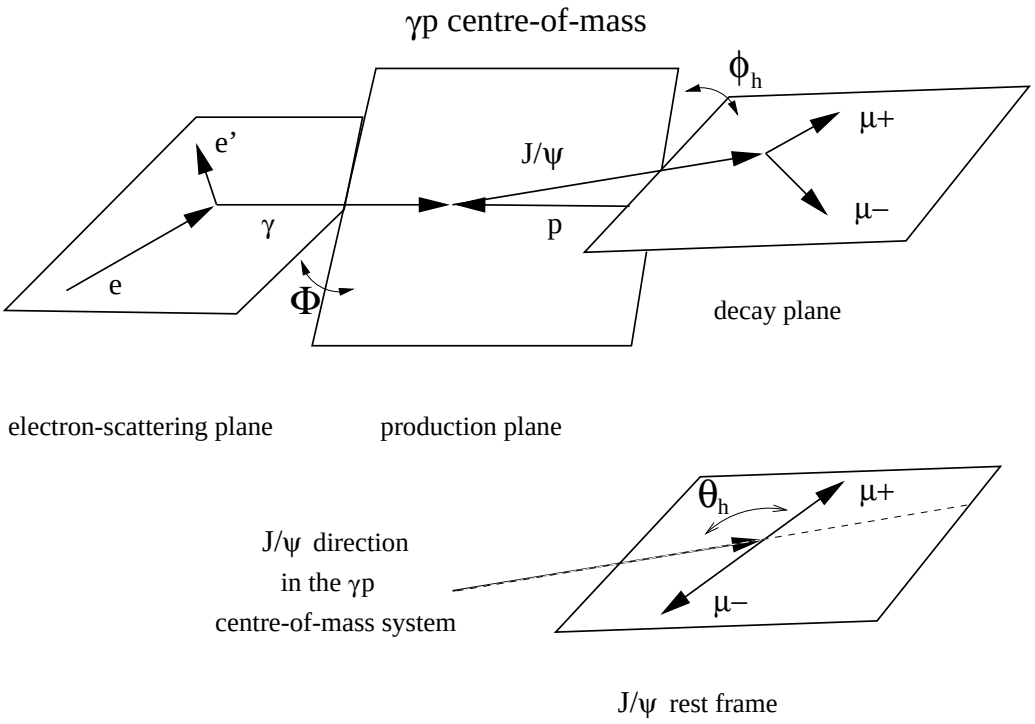

Figure 2: *Angles used to analyse the helicity states of the J/ψ, see text.*

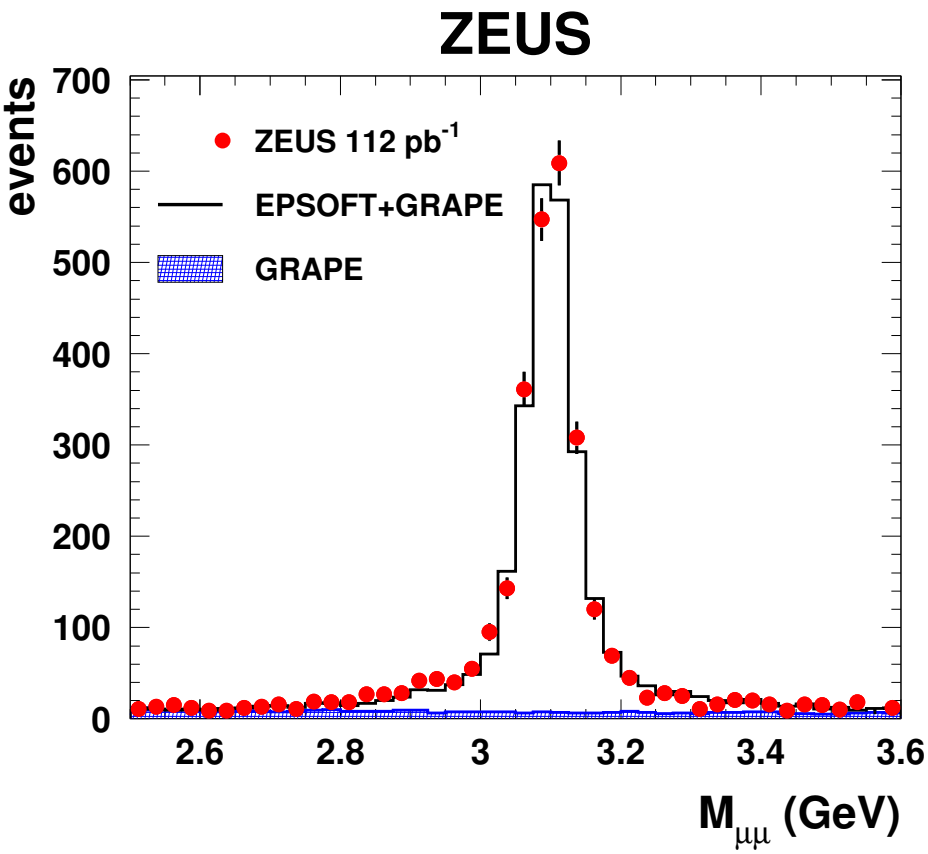

Figure 3: *The invariant-mass spectrum for $\mu^+\mu^-$ pairs in the range $30 < W < 160\,GeV$, $2 < |t| < 20\,GeV^2$ and $z > 0.95$. Error bars represent only statistical uncertainties. The data are compared to the MC distributions. The hatched histogram represents the $ep \to e\mu^+\mu^- Y$ background as simulated by the* GRAPE *MC. The solid-line histogram represents the sum of J/ψ and background MC events.*

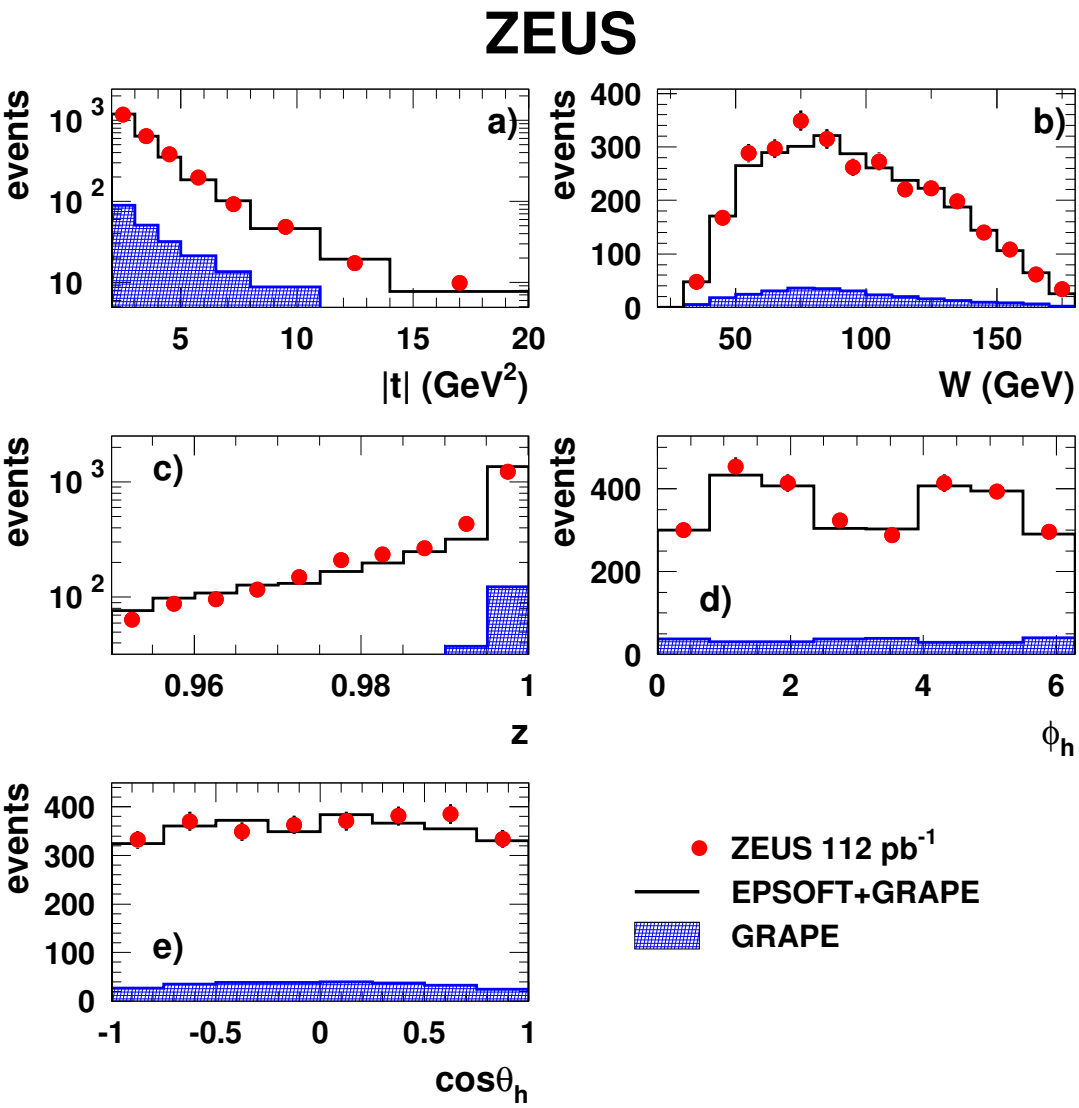

Figure 4: *Comparison between the data and MC distributions in the range* $30 < W < 160\ GeV$, $2 < |t| < 20\ GeV^2$ *and* $z > 0.95$ *for a)* $|t|$, *b)* W, *c)* z, *d)* ϕ_h, *e)* $\cos\theta_h$. *Error bars represent only statistical uncertainties. The hatched histograms represent the* $ep \to e\mu^+\mu^- Y$ *background as simulated by the* GRAPE *MC. The solid-line histogram represents the sum of* J/ψ *and background MC events.*

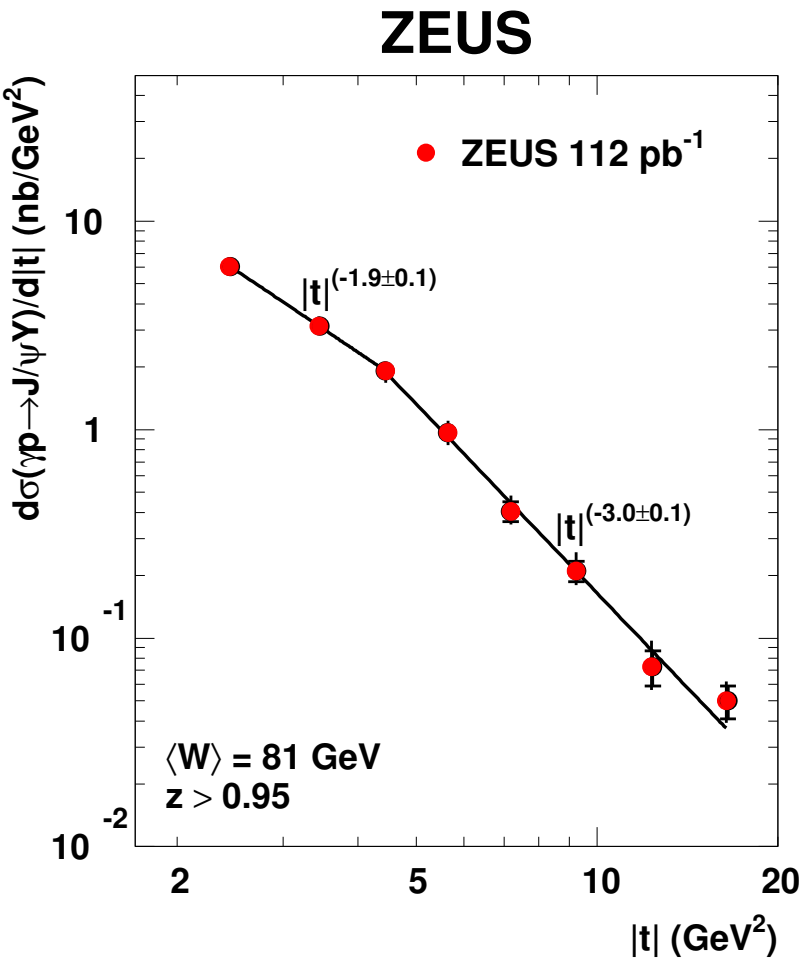

Figure 5: *The $|t|$ dependence of the differential cross-section $d\sigma/d|t|$ for the process $\gamma p \to J/\psi\, Y$ at $\langle W \rangle = 81\, GeV$ and $z > 0.95$. The inner bars correspond to the statistical uncertainties and the outer to the statistical and systematic uncertainties added in quadrature. The solid lines are the results of power fits to the form $d\sigma/dt \sim |t|^n$.*

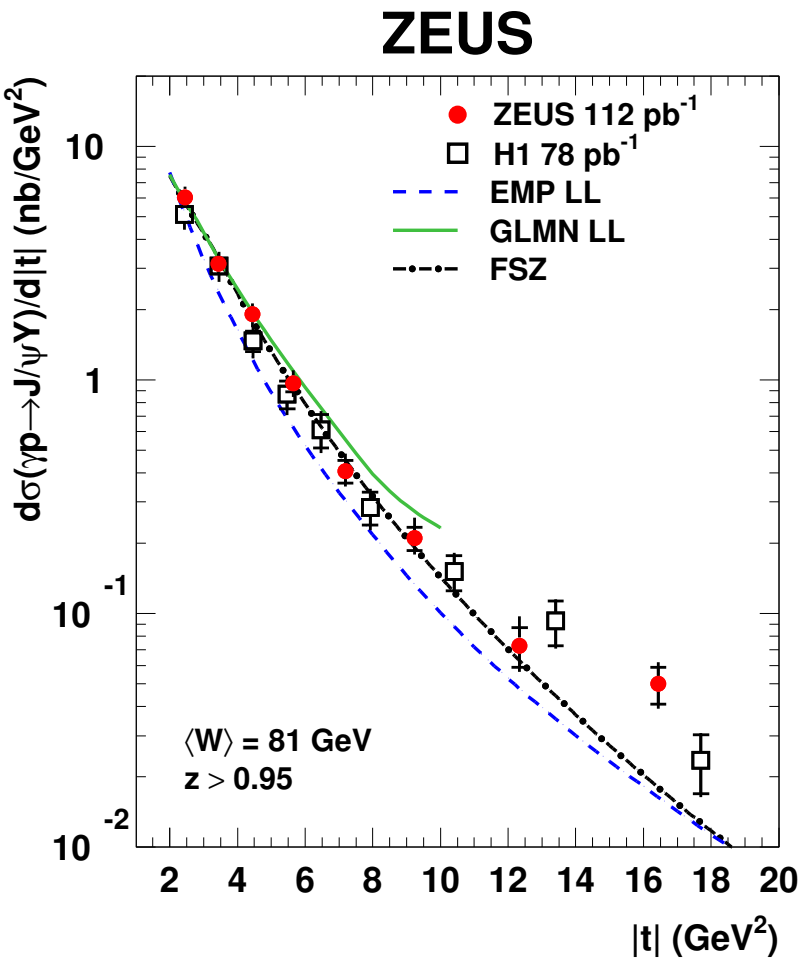

Figure 6: *The $|t|$ dependence of the differential cross-section $d\sigma/d|t|$ for the process $\gamma p \to J/\psi\, Y$ at $\langle W \rangle = 81\, GeV$ and $z > 0.95$. The H1 data, $50 < W < 150\, GeV$, [31] are also shown. The inner bars correspond to the statistical uncertainties and the outer to the statistical and systematic uncertainties added in quadrature. The lines show the predictions of several calculations, referred to in the text.*

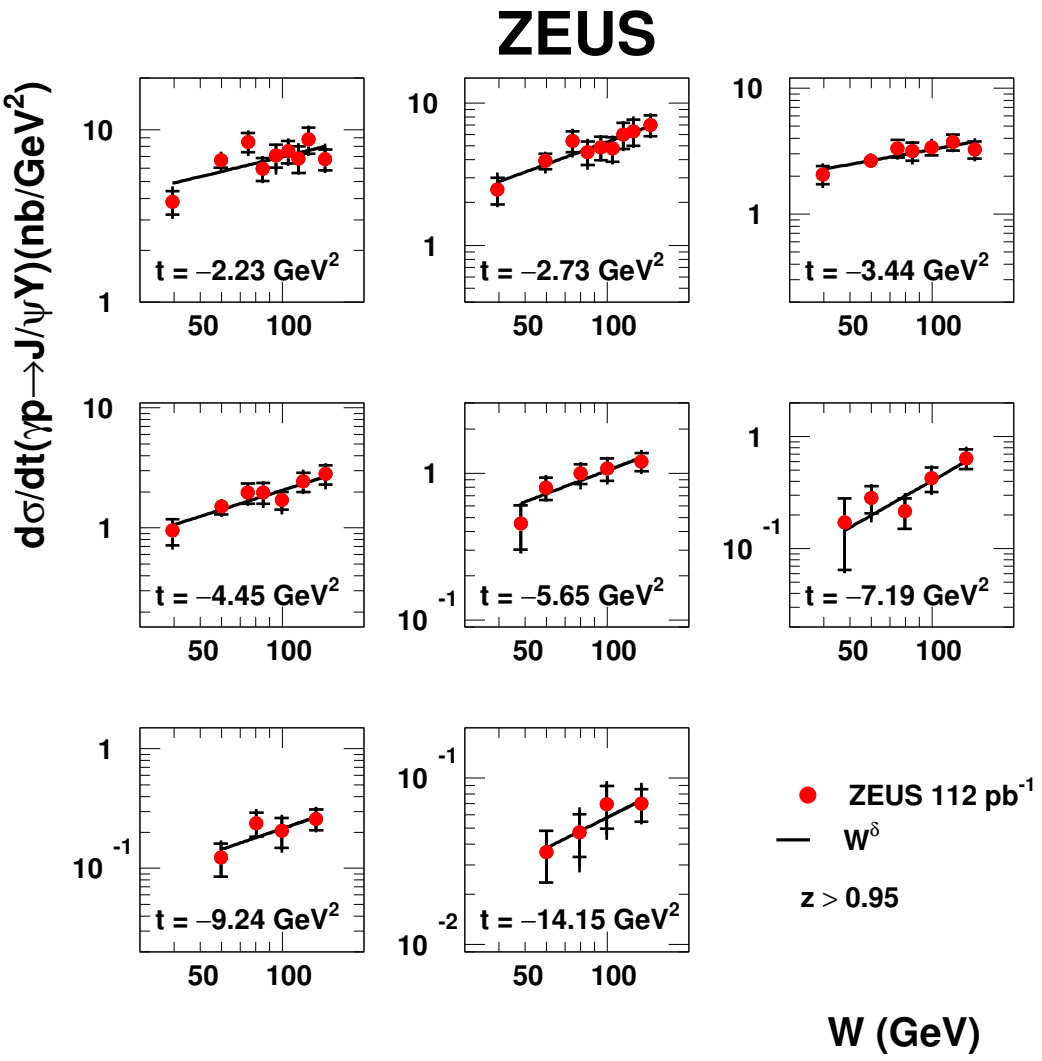

Figure 7: *The W dependence of the differential cross-section $d\sigma/dt$ for the process $\gamma p \to J/\psi\, Y$ ($z > 0.95$) at fixed $|t|$ values, as indicated in the figure. The inner bars correspond to the statistical uncertainties and the outer to the statistical and systematic uncertainties added in quadrature. The solid lines are the results of fits to the form $d\sigma/dt \sim W^{\delta}$.*

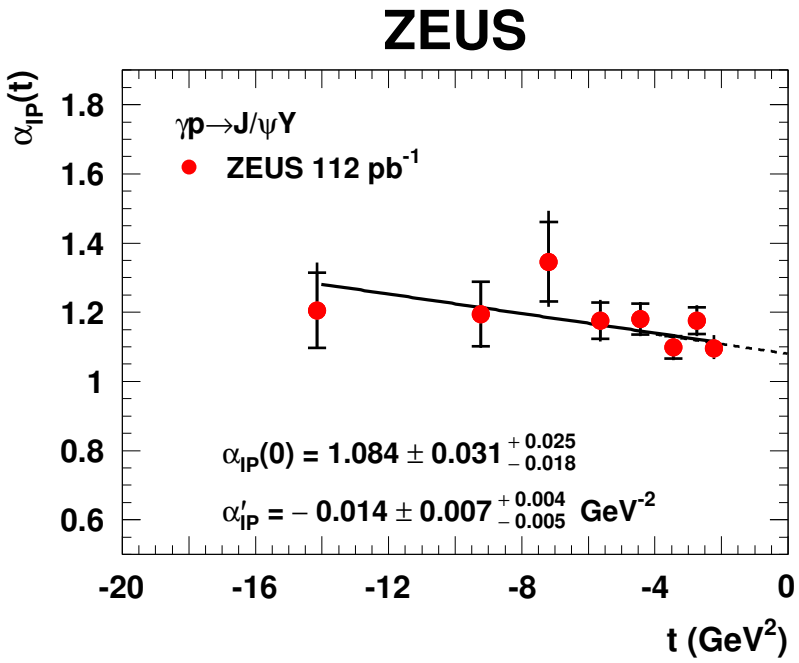

Figure 8: *The effective Pomeron trajectory as a function of t. The inner bars correspond to the statistical uncertainties and the outer to the statistical and systematic uncertainties added in quadrature. The solid line is a fit of the form $\alpha_{I\!P}(t) = \alpha_{I\!P}(0) + \alpha'_{I\!P} \cdot t$. The dashed line is an extrapolation to $\alpha_{I\!P}(0)$.*

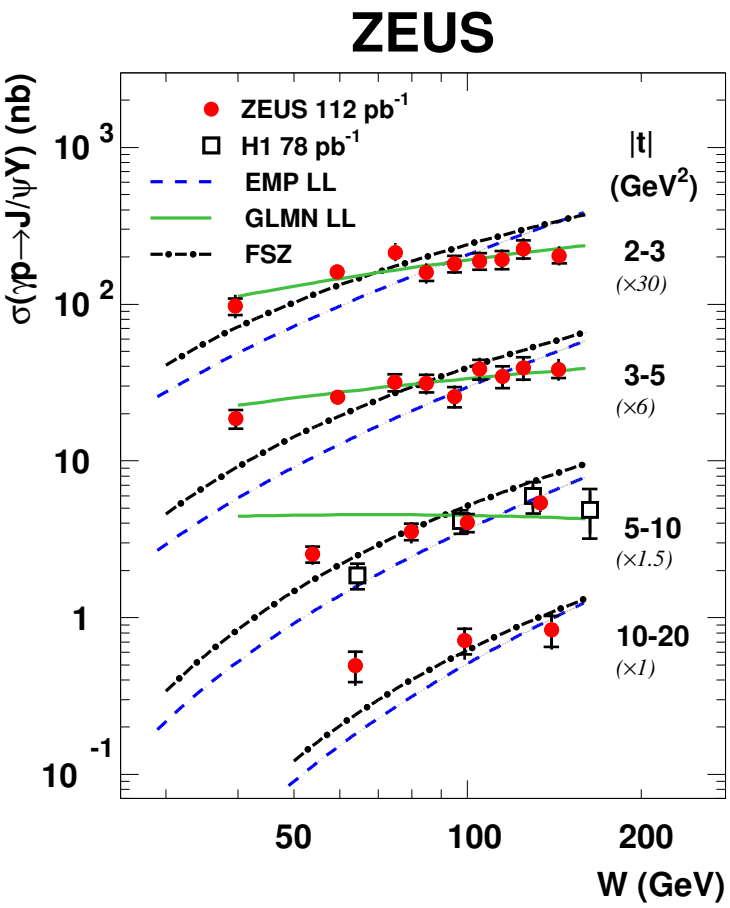

Figure 9: *The W dependence for the process $\gamma p \to J/\psi\, Y$ $(z > 0.95)$ in four different $|t|$ bins. The H1 data [31] for the $|t|$ bin of 5 to 10 GeV^2 are also shown. The inner bars correspond to the statistical uncertainties and the outer to the statistical and systematic uncertainties added in quadrature. The lines show the predictions of several calculations referred to in the text.*

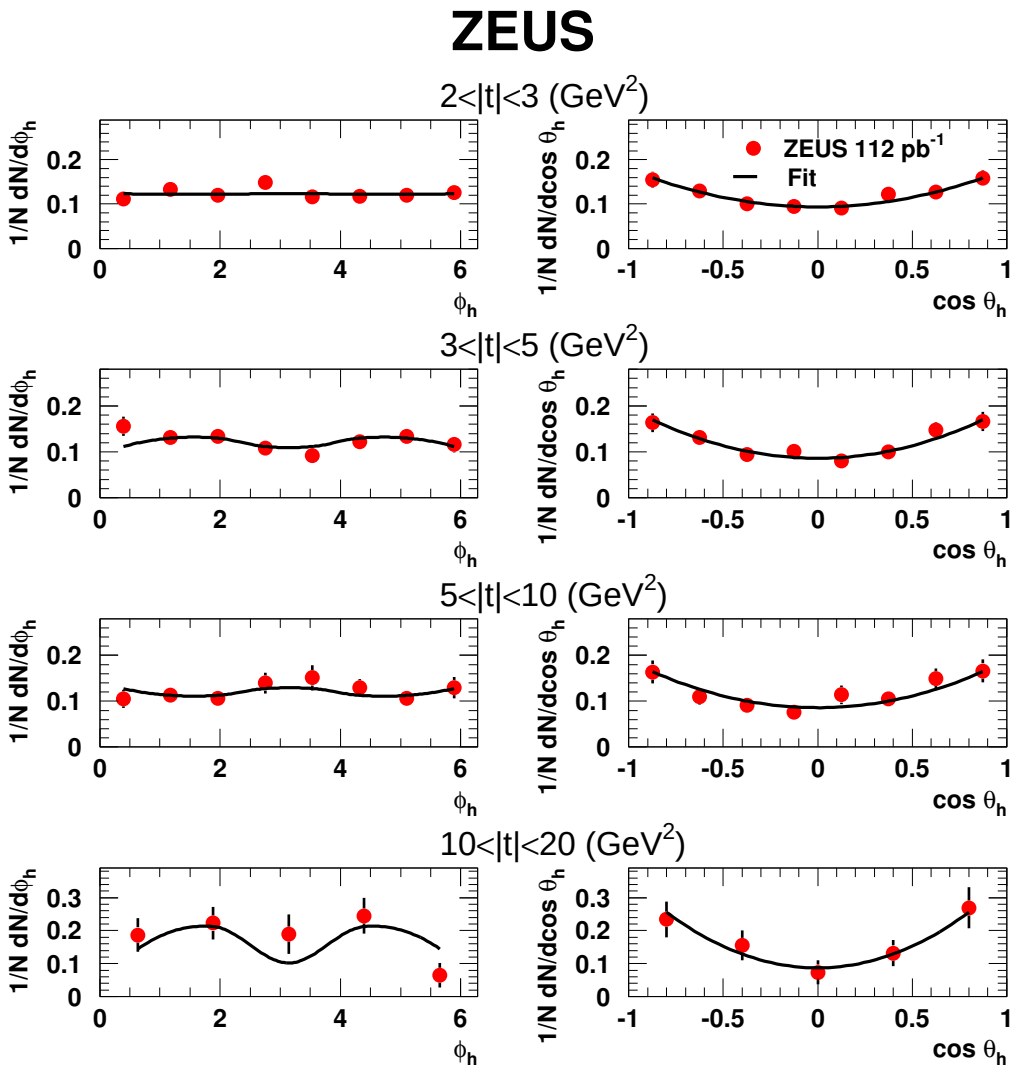

Figure 10: *The normalized distributions of ϕ and $\cos(\theta)$ for $30 < W < 160$ GeV and $z > 0.95$ in four bins of $|t|$. Error bars represent only statistical uncertainties. The lines represent the results of the fits according to formulae (8) and (9) in the text.*

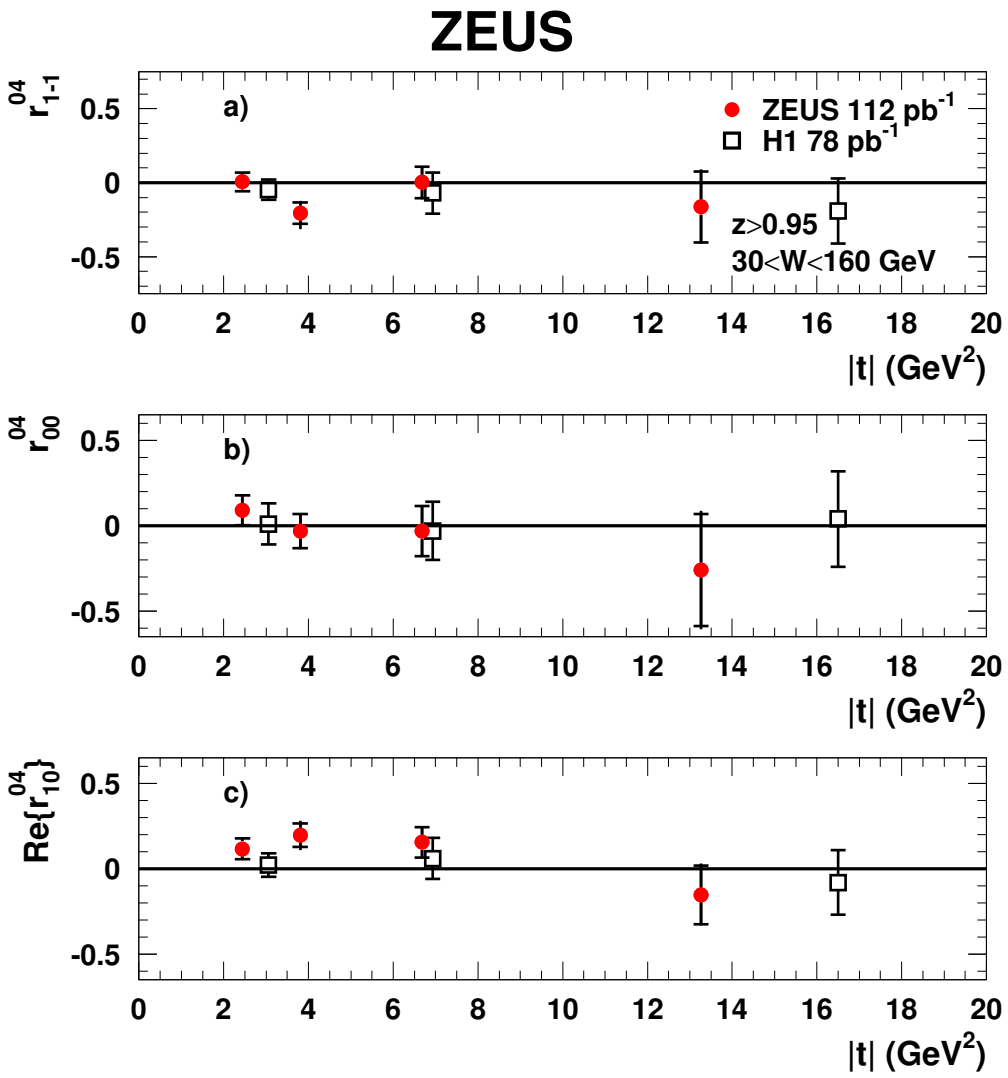

Figure 11: *Helicity spin density matrix elements a) r^{04}_{1-1}, b) r^{04}_{00} and c) $\mathrm{Re}\{r^{04}_{10}\}$ as a function of $|t|$ in the range $30 < W < 160\,GeV$ and $z > 0.95$. The H1 data, $50 < W < 150\,GeV$, [31] are also shown. The inner bars correspond to the statistical uncertainties and the outer to the statistical and systematic uncertainties added in quadrature. The solid lines show the expectation from SCHC.*